Evaluation of the Intranasal Flow Field through Computational Fluid Dynamics

Thomas Hildebrandt, MD[1] Leonid Goubergrits, DEng[2] Werner Johannes Heppt, MD[3] Stephan Bessler, MD[4] Stefan Zachow, DEng[5]

[1] Private practice of otorhinolaryngology in association with the Limmatklinik, Zurich, Switzerland
[2] Biofluid Mechanics Lab, Institute of Laboratory Medicine, Charité, Berlin, Germany
[3] Department of Otorhinolaryngology, Head and Neck Surgery, Staedtisches Klinikum Karlsruhe, Karlsruhe, Germany
[4] Private practice of otorhinolaryngology, Zurich, Switzerland
[5] Department of Scientific Visualization and Data Analysis, Zuse Institute, Berlin, Germany

Address for correspondence Thomas Hildebrandt, MD, private practice of otorhinolaryngology in association with the Limmatklinik, Hardturmstrasse 133, 8005 Zurich, Switzerland (e-mail: th@dr-hildebrandt.ch).

Facial Plast Surg 2013;29:93–98.

Abstract

A reliable and comprehensive assessment of nasal breathing is problematic and still a common issue in rhinosurgery. Impairments of nasal breathing need an objective approach. In this regard, currently rhinomanometry is the only standard diagnostic tool available but has various limitations. However, in the last decade, computational fluid dynamics (CFD) has become a promising method in facing the challenge of qualifying nasal breathing. This article presents use of CFD with a symptom-free subject and a symptomatic patient. Thereby, certain flow field features and changes before and after surgery were investigated. Moreover, the study outlines suggestions for concrete rhinologic CFD applications.

Keywords
- nasal resistance
- pressure drop
- nasal breathing
- flow field
- wall shear stress

Impairments of nasal breathing due to anatomical aberrations of the nasal framework are very common. One issue of their surgical treatment is to define and detect the core problem that has to be addressed.

It should be noted that nasal resistance is not strictly attributable to a certain geometry of the flow space. In other words, nasal resistance and the nasal cavity's morphologic configuration are not bijective. This might be the reason for some randomness in choosing the surgical target to improve nasal patency.

Currently, rhinomanometry is the clinical standard facilitating a certain objective approach to impairments of nasal breathing. However, even the most accurate measurement of the total nasal resistance is of limited informative value due to its integral character. Low resistance breathing cannot be equated with the occurrence of a physiologic airstream. This possibly explains, to some extent, the frequent disparities between patients' complaints and results of rhinomanometry. Bermüller et al published, for example, that ~ 25% of symptomatic patients with a functionally relevant nasal-structure deformity were not detected in a study.[1] Therefore, the German Society of Oto-Rhino-Laryngology assesses rhinomanometry as a useful tool in the preoperative diagnostic only in individual cases.[2]

In contrast, computational fluid dynamics (CFD) enables the calculation of various parameters of the intranasal flow field with a high temporal and spatial resolution that can also include the rhinomanometric value of the total nasal resistance as published in a recent study.[3] CFD is based on the physical principles of the conservation of mass, energy, and impulse that are summarized in a system of nonlinear partial differential equations known as Navier-Stokes equations. Numerical flow simulation is a well-established method of facing engineering problems. Increasingly, it becomes a valuable tool also in medicine to analyze blood or airflow.[4–9]

In this article, the employment of numerical flow simulation on the nasal breathing of a symptom-free subject and a symptomatic patient (pre- and postoperatively) is presented.

Issue Theme Innovations in Rhinosurgery; Guest Editor, Thomas Hildebrandt, MD

Copyright © 2013 by Thieme Medical Publishers, Inc., 333 Seventh Avenue, New York, NY 10001, USA. Tel: +1(212) 584-4662.

DOI http://dx.doi.org/10.1055/s-0033-1341591.
ISSN 0736-6825.

Objectives

The study aimed principally to outline features of the intranasal flow field that might be of special clinical relevance. Thereby, the focus was on the following parameters: velocity field, wall shear stress, and total pressure drop. They were considered in relation to various significant anatomical landmarks, namely, middle meatus, inferior turbinate, isthmus nasi, and the olfactory region.

This analysis was implemented through the investigation of a referential nasal geometry of a symptom-free subject on the one hand, presumed to be a benchmark providing physiologic airflow, and on the other hand, a nose that showed anatomical aberrations responsible for the patients' complaints in terms of impaired nasal breathing. The latter was primarily supposed to demonstrate the alignment of the surgically accomplished nasal breathing improvement with postoperative changes of the flow field.

Material and Methods

History and Data Acquisition

The Digital Imaging and Communications in Medicine data set of a symptom-free subject already existed. It was taken from a previous comprehensive CFD investigation performed in terms of a reference simulation of physiologic nasal airflow.[9–11] At that time, the data were derived from a helical computed tomography (CT) scan (Toshiba Aquilion 64; Toshiba, Nasu, Japan) with almost isotropic spatial resolution ($0.37 \times 0.37 \times 0.4$ mm). The scanned volunteer (male, 46 years of age) had no pathologic findings and therefore had normal nasal breathing in accordance with his regular rhinomanometry results. Shortly before the CT scan, a local decongestant (xylometazoline) was administered in combination with systemic application of methylprednisolone to create reproducible mucosa conditions and facilitate segmentation.

The symptomatic patient (male, 45 years of age) suffered from a chronic blocked nose without sensing a predominant side. In certain intervals, this was reinforced by extra congestion. The inspection of the nose revealed a septal deviation toward the left side within the isthmus area. Additionally, consecutive reactions of the inner lining of the ethmoidal cells were suspected. Therefore, he underwent a high resolution ($0.39 \times 0.39 \times 0.6$ mm) CT scan. In contrast to the asymptomatic subject, the mucosa was not medicinally decongested before the CT examination. The result confirmed the clinical diagnosis of a slight consecutive ethmoiditis. However, the primary cause of the nasal cavity's restricted ventilation seemed to be the septal deformity. The changes of the membranes in the ethmoid cells might have been secondary reactions.

The septum had to be straightened through an open rhinoplasty procedure with a so-called extracorporeal septoplasty.[12]

Six months after surgery, the patient was completely free of symptoms and the clinical examination showed a straight septum. The mucosa texture appeared to be enhanced. Due to the preoperative radiologic report of ethmoiditis, a control CT scan in a high-resolution mode ($0.39 \times 0.39 \times 0.6$ mm) was performed. It showed distinct improvement, but also residual spots in the ethmoid cells. Altogether, from the patient's and the medical point of view, there was no need for further treatment.

Geometric Models

Three-dimensional (3D) geometric models of the nasal cavities were reconstructed excluding the paranasal sinuses or ethmoidal cells and without the nostrils' surrounding inflow area due to the results of the previously mentioned numerical simulation that revealed a negligible effect of these structures on the intranasal flow field. The semiautomatic segmentation with subvoxel accuracy was performed using ZIB-Amira software (Zuse Institute, Berlin). Planar inlet and outlet surfaces were generated at the nostrils and the nasopharynxes. The latter were extended by a straight tube to improve the solution stability.

Finally, smoothed 3D geometric models of the nasal cavities of the symptom-free subject as well as the symptomatic patient, pre- and postoperatively, were available in a comparable comprehensiveness and quality.

Grid Generation

The nasal cavities were discretized, as is required for flow simulation, using tetrahedrons. Their total number varied in each geometric model between 2.7 and 2.8 million. The cells were generated from the triangulated surfaces consisting of $\sim$ 300,000 triangles with a node distance of 0.3 mm. This high mesh density allowed for resolution of small gaps with a minimum of five cells. The grid generation was executed using the preprocessor Gambit (ANSYS Inc., Canonsburg, PA), which provided high-quality meshes with a cell skewness below 0.75 and aspect ratios below 3.5. The mesh size used was sufficient to ensure a mesh-independent solution (as it was also shown in recent studies).[3,13]

Boundary Conditions

Employing the commercial CFD program Fluent 6.3.26 (ANSYS Inc.), a steady-state nasal airflow with a flow rate of 12 L/min and 21.4 L/min was simulated for inspiration and expiration. These values comply with the mean flow and the peak flow of a respiratory minute volume of 6 L/min in accordance with quiet nasal breathing when presuming a sinusoidal breathing cycle.

The following boundary conditions were applied: (1) rigid walls with "no slip" at all nasal walls, (2) a "pressure-outlet" condition with gauge pressure set to zero at the nostrils, and (3) an "inlet-velocity" condition with constant velocity resulting in the target flow rate in the extended nasopharynxes. The simulation setting allowed a solution with different flow rates in the left and right nasal cavities.

Physical and Mathematical Modeling

The air, with a density of 1.225 kg/m^3 and a dynamic viscosity of 1.789×10^{-5} kg/ms, was assumed to be incompressible due to the low Mach number (< 0.1). A quasi-steady flow condition is justified because the Strouhal number ($\mathrm{Sr} = L \times f/U$) was below 1, calculated with a mean flow velocity (U) of

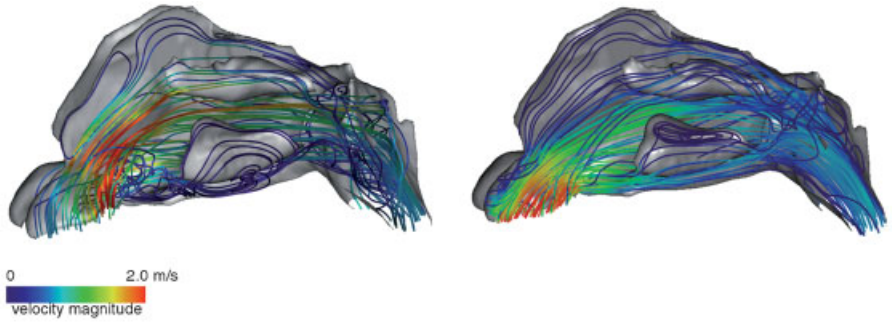

Fig. 1 Color-coded path lines of the symptom-free subject showing differences between inspiration (left) and expiration (right). Red means velocity magnitude of 2.0 m/s and higher.

0.7 m/s, a nasal airway length (*L*) of approximately 9 cm, and a breathing frequency (*f*) of 0.2 Hz.

Laminar flow was preconditioned because the laminar-turbulent transition refers to flow rates higher than 100 mL/s.[14]

Simulation and Visualization

The commercial program Fluent was applied in conjunction with a segregated solver using pressure-velocity coupling SIMPLEC and an upwind discretization scheme of the second order for the conservation laws. The convergence criterion of 10^{-5} was set for all residuals. The ZIB-Amira software was used for the analysis and visualization of the calculation results.

Results

Using the example of the symptom-free subject, certain general flow field features can be demonstrated, which, from our point of view, are of special clinical interest and to some extent have a representative character as they are also in accordance with other studies.

The velocity color-coded path lines displayed in ►**Fig. 1** show an "inspiratory jet" from the isthmus nasi into the middle meatus. The term *inspiratory jet* was recently used by Taylor et al.[15] An investigation by Sommer et al illustrated this phenomenon as significant regarding the lowered conditioning of the conducted air in this sector due to its velocity and amount.[16] Comparatively, the olfactory slit and the inferior meatus are less ventilated. This is supported by study results that show that only ~ 10% of the inhaled air reaches the olfactory area.[17,18] It is noticeable that, particularly at inspiration, there is a relatively high spatial disparity of the flow velocity within the nasal cavity (►**Fig. 1**).

In contrast, the simulation of expiration showed a more homogenous velocity distribution; for example, especially the inferior meatus and the inferior turbinate are exposed to enhanced convection and simultaneously, the flow velocity within the middle nasal passage is decreased (►**Fig. 1**).

As illustrated in ►**Fig. 2**, the consideration of the wall shear stress distribution revealed corresponding patterns.

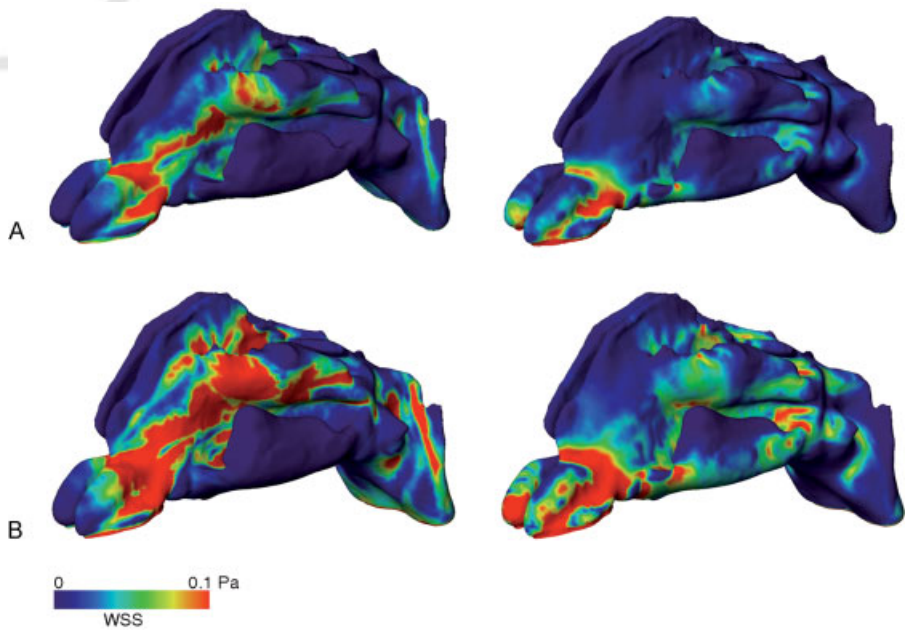

Fig. 2 Distributions of wall shear stress (WSS) in the symptom-free subject during inspiration (left) and expiration (right), calculated with mean flow (**A**) and peak flow (**B**).

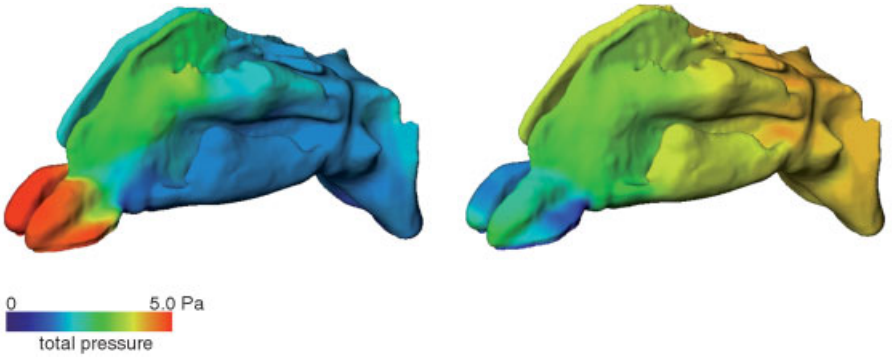

Fig. 3 Distributions of the relative total pressure during inspiration (left) and expiration (right) in the symptom-free subject.

At inspiration, a band of wall shear stress peaks ranges from the isthmus area mainly through the middle nasal passage, whereas the inferior turbinate and the olfactory region are exposed to less wall shear stress. This means that a comparatively low level of interaction or mass and heat transfer between the inner lining and the airstream takes place in these regions represented by the occurring wall shear stress. The low ventilation of the lateral inferior turbinate during inhalation was also reported by various other authors.[16,19–21]

At expiration, the wall shear stress level is altogether much lower and more balanced, but also with circumscribed wall shear stress peaks in the isthmus area. In contrast to inspiration, there is a rather equal distribution of wall shear stress within the nasal cavity. This assessment becomes more apparent if one considers a higher flow rate. Therefore, ►**Fig. 2** shows the mean flow (A) and the peak flow (B) simulation.

The visualization of the total pressure distribution, as displayed in ►**Fig. 3**, characterizing the pressure gradient in the nose, reveals a striking demarcation of the nasal vestibulum from the further posterior nasal cavity. It underlines the well-known fact that at this range, where the isthmus nasi is located, up to 80% of the total inspiratory nasal resistance originates.[22] In our investigation, the head of the inferior turbinate surprisingly does not contribute to this characteristic jump in the pressure drop, and therefore it might not be part of the isthmus nasi as it is frequently reported.[23,24]

The flow simulation of the symptomatic patient also revealed, in principle, the previously mentioned flow field characteristics of the symptom-free subject. However, the comparison of certain changes before and after surgery was of special interest in the symptomatic case.

A decline of the flow space constriction in the anterior part of the left nasal cavity (►**Fig. 4**) was obtained by the reconstruction of the isthmus nasi that resulted from the employed extracorporeal septoplasty. Therefore, the flow distribution between the two nasal cavities shifted from 56% right and 44% left to 53% right and 47% left, and the flow-normalized inspiratory resistances changed from 532 Pa min/m^3 right and 913 Pa min/m^3 left preoperatively to 618 Pa min/m^3 right and 776 Pa min/m^3 left postoperatively.

Not only the resistance on the right side but also the pressure drop or resistance of the entire nose surprisingly increased. The latter was ~ 16% higher after surgery than before, corresponding to a flow rate of 12 L/min considered at inspiration.

In this context, it should be noted again that the patient had no symptoms when he underwent the control CT scan. His subjective improvement of nasal breathing was supported by the changed total pressure distribution within the left nasal cavity and the different morphology of the left isthmus nasi displayed in ►**Fig. 4**. Their appearance before and after surgery approximated that of the primarily symptom-free subject (►**Fig. 3**) who was assessed as having undisturbed nasal breathing.

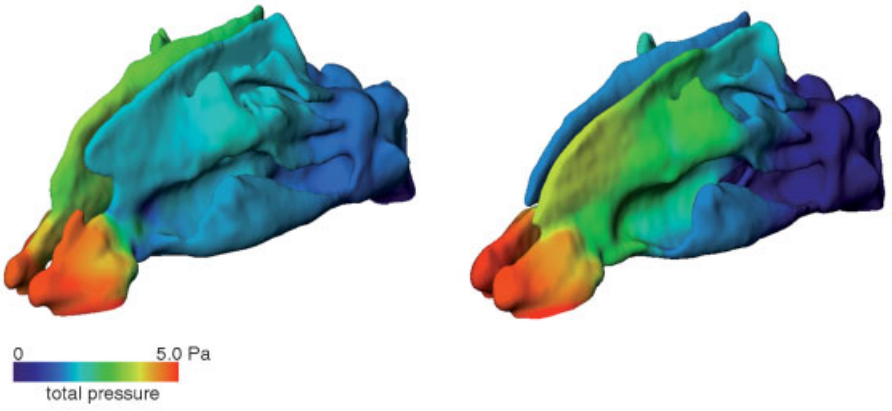

Fig. 4 Distributions of the relative total pressure during inspiration of the symptomatic patient, before (left) and after (right) surgery.

Discussion

The comparison of the inspiratory and expiratory flow field outlines that they are incongruent due to the nasal cavity's geometry. This is independent of the influence of the nasal valve at inspiration. The intranasal airstream course complies to some extent to those of a so-called Tesla valve,[25] which applies a different resistance to the fluid for each direction.

To speculate about the physiologic background, one could presume that this particular property of the nasal cavity is devoted to facilitating an appropriate heat and water balance in the nose in addition to constituting an adequate coupling between nasal breathing and the lung mechanics.[26]

The presented investigation suggests that the head of the inferior turbinate is, in contrast to the established opinion,[23,24] a rather minor contributor to the nasal isthmus resistance and is only involved to some extent in the mass and heat transfer from the inner lining to the inhaled air. However, the effect of its variant congestion on the pressure gradient or on the wall shear stress pattern was not of concern in this study. From our point of view, the inferior turbinate, with its large swelling capacity, is devoted foremost to ensuring a slitlike flow space.

Approximately 10% of the inhaled air is conducted to the olfactory region as already mentioned. This percentage is relatively independent of the flow rate.[18] In accordance with Taylor et al and Zachow et al, reduced wall shear stress and flow velocity were found in the olfactory cleft.[10,15] That means that sufficient residence time and a suitable milieu are provided for an efficient odor-receptor reaction or olfaction.

The isthmus nasi is a 3D structure consisting of several morphologic units,[24] and, therefore, it needs a 3D assessment that is not yet established. The sagittal constriction of the flow space in this area is widely neglected, although it probably has a distinctive effect as it is displayed by the pressure drop distribution (►**Figs. 3** and **4**).

The described inspiratory jet is supposed to cause a certain Venturi effect according to Bernoulli's law. This can disturb nasal breathing as the nasal valve is affected, although this commonly is only of clinical relevance for reinforced inspiration. Besides the impact on the elastic components of the nasal wall, the Venturi effect may contribute to the ventilation of the paranasal sinuses as the ostium or hiatus semilunaris and the inspiratory jet, consisting of fast-flowing air, meet in the middle nasal passage. This active pulsating extra ventilation force during breathing might prevent chronic or recurrent sinusitis. However, Fiedler showed that there is no noticeable increase in the frequency of sinusitis when nasal breathing is eliminated by laryngectomy.[27] Additionally, one could suggest that this mechanism also supports the release of nitric oxide from the maxillary sinus, where it is of high concentration (3,000 to 25,000 parts per billion).[28] But it was shown that only approximately 12% of the nasal nitric oxide originates from the paranasal sinuses.[28]

The study results of the symptomatic patient demonstrate once more that the consideration of the total nasal resistance is only of relative value. After surgery, the patient was symptom-free and had no complaints about nasal breathing, although the simulation revealed an increase of the total nasal resistance. This documents, to some extent, that the nasal resistance might not be sufficient to qualify nasal breathing as is the experience with patients with empty nose syndrome. Apparently, the complex interdependency of two parallel flow-depending resistances caused, in the presented case, a seemingly paradoxical result that is not clinically predictable.

Conclusion

The presented study illustrates, among other things, why the isthmus nasi is of great importance. This area needs particular attention in the diagnosis of nasal breathing impairments and their surgical treatment. Especially, its sharp demarcation in the visualized pressure drop distribution clarifies our experience that even a rhinoscopically, almost unnoticeable, septal deviation can be the actual reason for an apparently unexplainable impairment of nasal breathing.

In the past, we complemented the diagnosis of nasal breathing problems by regularly practicing bidigital palpation of the caudal septum. Subsequently, we are employing the extracorporeal septoplasty through an open approach more frequently, which, in our opinion, provides the best accuracy in the crucial isthmus area.[12,29] The numerical flow simulation provides an additional confirmation of the value of this surgical concept.

It should be noted that the rigidity of the septum might also be of significance, and not only for structural reasons. A missing cartilage in the isthmus area, as can partially occur in case of the L-span reconstruction technique, implies the possibility of a blockage of one nasal cavity during inspiration due to the Venturi effect.

The necessity of a 3D view on the nasal isthmus suggests CFD application as a tool to analyze isthmus deformities and align anatomical structures with the functional isthmus of the nasal cavity.

CFD also enables addressing the dynamic of the two interacting intranasal flow fields that, in our opinion, are underestimated in functional rhinosurgery but difficult to understand intuitively. Thus, CFD can help to put more rhinologic focus on this common issue of fluid dynamics.

The contradictory results regarding the role of the inferior turbinate suggest further investigations should be done using CFD.

Acknowledgments

We are grateful to Jan Osman, BSc, for supporting the CFD preprocessing.

References

1 Bermüller C, Kirsche H, Rettinger G, Riechelmann H. Diagnostic accuracy of peak nasal inspiratory flow and rhinomanometry in functional rhinosurgery. Laryngoscope 2008;118:605–610

2 Mlynski G, Beule A. Diagnostik der respiratorischen Funktion der Nase [Diagnostic methods of nasal respiratory function]. HNO 2008;56:81–99

3 Kimbell JS, Garcia GJM, Frank DO, Cannon DE, Pawar SS, Rhee JS. Computed nasal resistance compared with patient-reported symptoms in surgically treated nasal airway passages: a preliminary report. Am J Rhinol Allergy 2012;26:e94–e98
4 Doorly DJ, Taylor DJ, Gambaruto AM, Schroter RC, Tolley N. Nasal architecture: form and flow. Philos Transact A Math Phys Eng Sci 2008;366:3225–3246
5 Doorly DJ, Taylor DJ, Schroter RC. Mechanics of airflow in the human nasal airways. Respir Physiol Neurobiol 2008;163:100–110
6 Elad D, Naftali S, Rosenfeld M, Wolf M. Physical stresses at the air-wall interface of the human nasal cavity during breathing. J Appl Physiol 2006;100:1003–1010
7 Goubergrits L, Schaller L, Kertzscher U, et al. Statistically wall shear stress maps of ruptured and unruptured middle cerebral artery aneurysms. J R Soc Interface 2012;69:677–688
8 Goubergrits L, Wellnhofer E, Kertzscher U, Affeld K, Petz C, Hege H-C. Coronary artery WSS profiling using a geometry reconstruction based on biplane angiography. Ann Biomed Eng 2009;37:682–691
9 Zachow S, Steinmann A, Hildebrandt T, Weber R, Heppt W. CFD simulation of nasal airflow: towards treatment planning for functional rhinosurgery. Int J Comput Assist Radiol Surg 2006;1 (S1):165–167
10 Zachow S, Muigg P, Hildebrandt T, Doleisch H, Hege H-C. Visual exploration of nasal airflow. IEEE Trans Vis Comput Graph 2009;15:1407–1414
11 Zachow S, Steinmann A, Hildebrandt T, Heppt W. Understanding nasal airflow via CFD simulation and visualization. In: Proc Computer Aided Surgery around the Head. Berlin: Pro Business Verlag; 2007:173–176
12 Gubisch W. Twenty-five years experience with extracorporeal septoplasty. Facial Plast Surg 2006;22:230–239
13 Zhu JH, Lee HP, Lim KM, Lee SJ, Teo Li San L, Wang DY. Inspirational airflow patterns in deviated noses: a numerical study. Comput Methods Biomech Biomed Engin 2012
14 Doorly DJ, Taylor DJ, Gambaruto AM, Schroter RC, Tolley N. Nasal architecture: form and flow. Philos Transact A Math Phys Eng Sci 2008;366:3225–3246
15 Taylor DJ, Doorly DJ, Schroter RC. Inflow boundary profile prescription for numerical simulation of nasal airflow. J R Soc Interface 2010;7:515–527
16 Sommer F, Kröger R, Lindemann J. Numerical simulation of humidification and heating during inspiration within an adult nose. Rhinology 2012;50:157–164
17 Delank KW. Aerodynamik im Bereich des Riechorgans. In: Stoll W, ed. Klinik der menschlichen Sinne. Wien, Austria: Springer Verlag; 2008:50–58
18 Keyhani K, Scherer PW, Mozell MM. Numerical simulation of airflow in the human nasal cavity. J Biomech Eng 1995;117: 429–441
19 Hahn I, Scherer PW, Mozell MM. Velocity profiles measured for airflow through a large-scale model of the human nasal cavity. J Appl Physiol 1993;75:2273–2287
20 Proctor DF. The upper airway. In: Proctor DF, Anderson IB, eds. The Nose. Upper Airway Physiology and the Atmospheric Environment. New York, NY: Elsevier, Urban & Fischer; 1982:23–43
21 Wen J, Inthavong K, Tian ZF, Tu JY, Xue CL, Li CG. Airflow Patterns in Both Sides of a Realistic Human Nasal Cavity for Laminar and Turbulent Conditions. Paper presented at: 16th Australasian Fluid Mechanics Conference; December 3–7, 2007; Gold Coast, Australia
22 Wexler DB, Davidson TM. The nasal valve: a review of the anatomy, imaging, and physiology. Am J Rhinol 2004;18:143–150
23 Huizing EH, De Groot JAM. Functional Reconstructive Nasal Surgery. 1st ed. Stuttgart, Germany: Thieme; 2003:47–50
24 Bloching MB. Disorders of the nasal valve area. GMS Curr Top Otorhinolaryngol Head Neck Surg 2007;6:Doc07
25 Tesla N. Valvular Conduid. US-Patent 1329559 (1920)
26 Hildebrandt T. Das Konzept der Rhinorespiratorischen Homöostase—ein neuer theoretischer Ansatz für die Diskussion physiologischer und physikalischer Zusammenhänge bei der Nasenatmung [PhD dissertation]. Freiburg im Breisgau, Germany: Albert-Ludwigs-Universität; 2011
27 Fiedler G. Retrospektive Analyse sinunasaler Erkrankungen bei 104 Patienten nach Laryngektomie [PhD dissertation]. Marburg, Germany: Phillips-Universität; 2008
28 Maniscalo M, Lundberg JO. Nasal nitric oxide. Eur Respir Mon 2010;49:71–81
29 Heppt W, Gubisch W. Septal surgery in rhinoplasty. Facial Plast Surg 2011;27:167–178